ELSEVIER

Journal of Nuclear Materials 266–269 (1999) 207–216

journal of nuclear materials

Conclusions about the use of tungsten in the divertor of ASDEX Upgrade

K. Krieger *, H. Maier, R. NeuASDEX Upgrade Team

Max-Planck-Institut für Plasmaphysik, IPP-EURATOM Association, Boltzmannstraße 2, D-85748 Garching, Germany

Abstract

Tungsten divertor plates have been used in ASDEX Upgrade for a full experimental campaign of approximately 800 discharges. Key issues investigated were the plasma performance, tungsten erosion, redeposition and migration, hydrogen isotope retention and the consequences of the simultaneous use of carbon and tungsten as plasma facing materials. Tungsten behavior was investigated by spectroscopic observation of line and quasi-continuum radiation and by surface analysis of material probes and of samples taken from plasma facing components after the experimental campaign. Code simulations were used to gain further understanding of the observed tungsten erosion properties and of tungsten plasma transport processes. The results obtained so far are presented and the implications with respect to the construction of future fusion devices are discussed.

Keywords: ASEX-Upgrade; Deuterium inventory; Erosion/deposition; High-Z material; impurity transport; Tungsten

1. Introduction

The use of high-Z materials in fusion devices was discouraged by early results obtained with the PLT tokamak, which was equipped with a tungsten limiter [1,2]. Because of the direct contact of the limiter with the hot plasma edge, the energy of the impacting plasma ions exceeded the tungsten sputtering threshold energy. This led to significant tungsten contamination of the core plasma with corresponding strong degradation of plasma performance. Similar results showing accumulation of tungsten in the plasma core for a limiter source under certain discharge conditions were also found in TEXTOR recently [3,4]. Consequently, low-Z materials (e.g. Be, C) have been adopted for the plasma facing components of most fusion experiments.

On the other hand, in the divertor region of a fusion device with ignited plasma, high particle fluxes of low energies will severely degrade the lifetime of plasma facing components made of low-Z materials. Under such conditions high-Z materials, in particular tungsten, are considered as a favourable option, primarily due to their low sputtering yield and their high sputtering threshold energy.

To examine the feasibility of tungsten as a material for plasma facing components in the divertor region, ASDEX Upgrade was equipped with W-coated divertor plates for a full experimental campaign. Major points of interest were the study of tungsten erosion, migration and redeposition processes as well as the influence of the eroded tungsten on plasma performance. Since the remaining plasma facing components still consisted of carbon materials, it was also possible to investigate for the first time the interaction of low-Z main chamber walls with high-Z divertor components under reactor relevant plasma conditions. Finally, detailed studies of hydrogen isotope retention at the tungsten tiles were carried out and the results were compared to those obtained for the previously installed graphite tiles.

Initial results on tungsten erosion and migration have been reported in [5–10]; first results on plasma performance have been presented in [11,12]. In the following, the results on plasma wall interaction effects such as erosion, global migration, redeposition, hydrogen isotope retention and the interaction of the tungsten divertor with carbon main chamber walls will be

* Corresponding author. Tel.: +49 89 32 99 1655; fax: +49 89 32 99 1149; e-mail: krieger@ipp.mpg.de

0022-3115/99/$ – see front matter
PII: S0022-3115(98)00890-3

summarized. Details on tungsten transport and radiation in the main plasma will be presented in a separate forthcoming publication [13].

2. The tungsten divertor

The tungsten divertor was introduced in the Divertor I configuration of ASDEX Upgrade and consisted of toroidal belts of tungsten coated graphite tiles on the inner and outer divertor plate at the respective strike point zones as shown in Fig. 1. Customized graphite tiles covering less than 10% of the total area had to be left for Langmuir probes, thermography and a probe manipulator. At less exposed areas the original graphite tiles were kept in use as well.

To avoid hot spots at the upstream edges, the tile surfaces were manufactured with a slight inclination of 1.1° to the horizontal plane in toroidal direction. This resulted in approximately 20 mm of the tile surface being shaded from the incident plasma in toroidal direction at the cost of a 30% increased heat flux density to the plasma wetted area compared to horizontal tile surfaces.

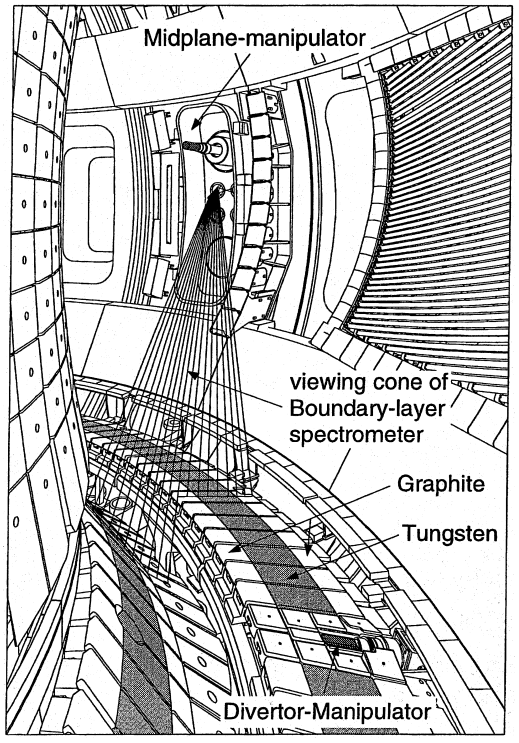

Fig. 1. Perspective view into the ASDEX Upgrade vacuum vessel showing the mid-plane and the divertor probe manipulator systems with probes at the respective exposure positions. The typical BLS radial scan range across the divertor is illustrated by a set of respective viewing chords.

As a result of preceding material tests with prototypes, the tungsten tiles were manufactured by plasma spray coating of graphite tiles. Detailed results on these tests, and on the structure and manufacturing process of the tiles have been described elsewhere [14,15]. Within the tungsten divertor campaign, ≈800 plasma discharges were carried out with average heat loads of up to 6 MW/m^2 and peak loads during ELMy H-Mode discharges of up to 15 MW/m^2. After termination of the experimental campaign, cracks were found on most of the tungsten coated tiles. The width of the cracks was, in accordance with results from preceding beam irradiation tests with similar cycling heat load, too small to cause formation of hot spots. Consequently, no influence on the measured W-concentrations in the core plasma and on the plasma performance was observed [11,12]. Detailed results on the tiles' technical performance in the tungsten campaign, in particular with respect to the morphology of the crack patterns, are reported in Ref. [16].

3. Plasma performance and tungsten concentration

Global plasma parameters like energy confinement, β-limit, density limit and H-mode threshold remained unchanged from previous experimental campaigns with graphite tiles used for the divertor plates [11,12]. Furthermore, replacing the graphite target tiles with tungsten tiles had no significant impact on the concentration of carbon [12]. This indicates that the graphite divertor did not contribute significantly to the carbon plasma contamination. Consequently, the carbon source must be attributed predominantly to erosion of other plasma facing components such as the inner heat shield and carbon limiters in the main chamber. Spectroscopic observation of the inner heat shield shows indeed a significant carbon flux proportional to the hydrogen recycling flux [17].

Tungsten concentrations in the confined plasma were determined by spectroscopic observation of tungsten emission lines and of tungsten quasi-continuum radiation, depending on the plasma temperature [18]. Detailed laser ablation experiments had been carried out to identify appropriate spectral lines of the predominant tungsten charge states [18–20]. In 85% of the discharges, the tungsten concentration in the core plasma remained below 2×10^{-5}, which is considered to be the acceptable upper limit for ITER operation. Consequently, no increase of the central radiation was observed from previous experimental campaigns.

The tungsten concentration decreased strongly with increasing density [13]. Correlation with neutral beam heating power was not as strong, however, a decrease of the maximum W-concentration was observed with increasing heating power [11,12]. Discharges where the observed W-concentrations significantly exceeded the

limit of 2×10^{-5} can be categorized into three distinct types: discharges with counter neutral beam injection, discharges featuring strongly peaked density profiles and discharges with low energy neutral beam heating [13]. These scenarios are characterized by an overall accumulation of impurities, which is well known from observations in earlier tokamak experiments [21,22] and therefore the above result is not peculiar to the presence of tungsten in the machine. Apart from accumulation scenarios, increased tungsten confinement was also observed in a few discharges due to trapping of tungsten in magnetic islands [18], however, with core concentrations still within the acceptable range. The dominant influence of plasma transport processes on the observed W-density is illustrated by Fig. 2, which shows the W-density in the central region of the main plasma as a function of the effective tungsten source flux at the outer divertor plate for different discharge scenarios. There is no significant correlation between W-source and W-plasma density. Moreover at a given W-source flux the observed W-density varies over up to 3 orders of magnitude with the accumulation scenarios featuring the highest values. In contrast, the W-density in Ohmic discharges was below the detection limit in most cases regardless of the W-source flux.

Studies of tungsten cross-field transport coefficients [23] showed that collisional W-transport is dominated by carbon–tungsten collisions. The main contribution to the tungsten neoclassical drift velocity is given by terms proportional to the temperature gradient of the carbon ions. For typical plasma density and temperature profiles, the resulting tungsten drift velocities outside the central region are directed outwards, resulting in hollow W-concentration profiles. The predicted increase of the outward drift with increasing carbon density is in qualitative agreement with the observed anti-correlation of W-density and carbon density [23].

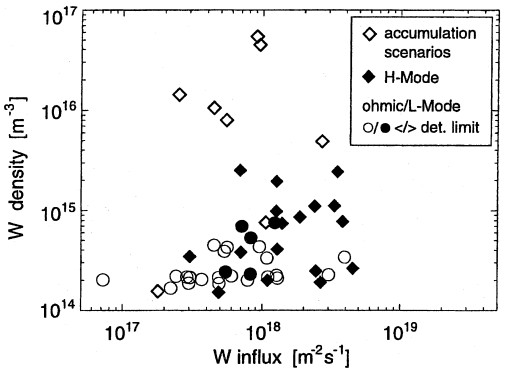

Fig. 2. Tungsten density in the confined plasma as a function of the effective tungsten source flux at the outer divertor plate. The effective source flux was derived from the spectroscopically determined total flux by subtracting the fraction of promptly redeposited ions. Open circles denote the upper limit of the tungsten density in cases where the tungsten density was below the detection limit.

4. Erosion and local redeposition

The total flux of sputtered tungsten atoms was measured by observation of tungsten line emission [9] using the ASDEX Upgrade Boundary Layer Spectrometer (BLS) [24]. By means of a rotatable swivel mirror, the instrument is capable of recording spatial profiles of line emission in the visible as well as in the VUV range. A typical poloidal scan range across the divertor plates is shown in Fig. 1.

Spectral lines of W-atoms and of singly charged W-ions had been identified at the PSI-1 plasma generator at IPP/Berlin [25]. For the most prominent WI-line at 400.8 nm the photon efficiency S/XB was determined as a function of electron temperature T_e by measuring the ratio of W-erosion flux to the corresponding WI photon flux at a tungsten target exposed in stationary plasma discharges of the PSI-1 device [26]. The erosion flux was obtained from the weight loss of the target. At electron temperatures above the PSI-1 limit of 20 eV, S/XB was determined similarly in ASDEX Upgrade by sublimation of $W(CO)_6$ into the outer divertor plasma using an oven probe [27], which was exposed at the outer target plate by means of a divertor manipulator system (Fig. 1).

For the interpretation of the measured erosion flux, the particle flux onto the target plates, Γ_D, and the energy of the incident particles must be known. Interpretation of spectroscopic observations requires in addition electron density n_e and temperature T_e above the target surface. Direct measurement of these parameters is provided by a set of flush mounted Langmuir probes mounted at various radial positions in the target plates [28]. Alternatively, the particle flux was computed from the heat flux to the target plate in combination with the Langmuir-T_e data.

Fig. 4(b) shows the distribution of the WI line emission across the outer divertor plate recorded by a radial scan of the BLS line of sight during the stationary phase of an Ohmic discharge [9]. The radial profile of the WI intensity is characterized by two distinct maxima, which reflect the convolution of temperature and plasma ion flux at the target [Fig. 4(a)]. The maximum close to the strike point corresponds to the peak value of the temperature while the right hand maximum is due to the corresponding increase of the particle flux. From the close correlation of the WI intensity to Γ_D and T_e we conclude that the erosion is indeed determined mainly by these parameters. Furthermore, the result shows that WI emission is localized closely above the target plate and that migration in radial direction can be neglected,

which is a necessary condition for the derivation of the erosion flux from the measured photon flux. Further evidence for localized emission is given by the steep decrease of the WI signal at the outer edge of the W-tile towards the adjacent graphite tile.

The WI intensity was found to increase strongly with increasing neutral beam heating power due to the corresponding increase of particle flux and plasma temperature at the target plates. On the other hand increasing the plasma density at constant heating power leads to lower divertor temperatures and correspondingly to a strong decrease of WI emission [9,12].

Assuming constant T_e in the WI emission zone it is possible to compute the tungsten erosion flux from the WI photon flux and the photon efficiency. The ratio of tungsten flux to deuterium flux represents the tungsten sputtering yield, Y. Fig. 3 shows the yield as a function of T_e at the target plate. The data were derived from Ohmic as well as from auxiliary heated discharges. It should be noted that the data at higher temperature were derived mainly from H-mode discharges where the plasma conditions in the divertor are no longer stationary due to periodic heat and particle pulses delivered to the target plates by ELMs. Within an ELM pulse the plasma temperature at the target can reach values exceeding 50 eV. Since typical type I ELM frequencies are in the range of 50–500 Hz, the observed WI radiation represents in this case a time average over many ELM periods because of the comparatively low acquisition rate of the BLS detector.

The average yield is determined to a large extent by erosion within the ELMs and therefore depends not only on the ELM temperature but also on the ELM repetition frequency, which increases with heating power. This is taken into account by plotting the respective yields as a function of the temperature averaged over the spectrometer exposure time.

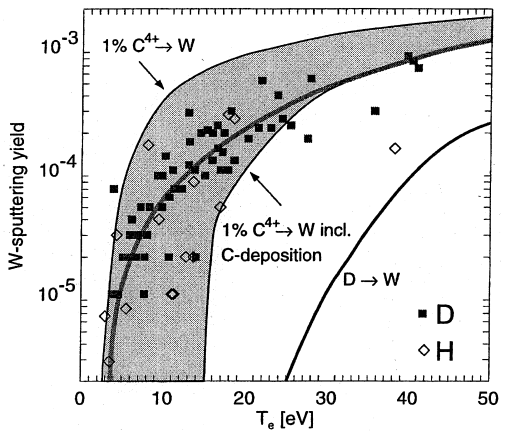

Fig. 3. Sputtering yield of tungsten as function of T_e at the target plate computed from the WI line emission. The solid lines represent sputtering yields calculated by TRIM simulation for deuterium and carbon as bombarding particles.

Sputtering yields measured in hydrogen and deuterium plasmas showed no significant difference. The measured yields were further compared to results of TRIM sputtering simulations assuming bombardment of tungsten by deuterium ions with a Maxwellian energy distribution including the additional acceleration in the sheath potential [29]. As illustrated by Fig. 3 the calculated sputtering yields for deuterium impact on tungsten are much lower than the experimental results. From these observations we conclude that the contribution of the plasma ions to tungsten erosion is negligible in the temperature range covered by the measured data (<50 eV). On the other hand, low-Z impurity ions in the plasma will reach the target plates typically with charge states 3+ and more. Due to the corresponding additional acceleration in the sheath potential and due to their higher mass they can be expected to completely dominate tungsten sputtering. This is in good agreement with TRIM simulations assuming simultaneous sputtering by deuterium and an additional fraction of multiple charged C ions [29]. In this case one has to take into account that the impacting C-ions will be implanted into the W-surface leading to a gradual decrease of the tungsten surface concentration until a stationary level is reached where the carbon deposition is balanced by erosion. Below a certain threshold temperature, which increases with carbon plasma concentration, there will be net deposition of carbon leading to the formation of a protective layer on top of the W-surface and correspondingly vanishing tungsten erosion [30]. Fig. 3 shows the calculated yield in the stationary limit including the effect of carbon deposition for a plasma concentration of 1% C^{4+} ions. The measured yields are still larger. A closer match with the simulations can be achieved if a carbon fraction of 0.7% is assumed. Without inclusion of the deposition effects, the calculated erosion is too large as illustrated in Fig. 3.

The net erosion flux integrated over one discharge or a series of subsequent discharges was determined by measuring ex situ the erosion of material probes exposed at the strike point zone of the outer deviator plate [5] using the manipulator system shown in Fig. 1. By means of vapor deposition graphite probes were covered with thin (1–100 nm) tungsten marker stripes oriented in radial direction. The thickness of the stripes in terms of the atom area density was measured before and after exposure by Rutherford backscattering analysis using 700 keV ^{4}He.

Fig. 4(c) shows a radial profile of the W-erosion across the outer divertor plate measured in a series of low density Ohmic discharges. The data are strongly correlated to the spatial distribution of the WI emission during the stationary phase of the discharges [Fig. 4(b)]. The small discrepancy at the left of the strike-point

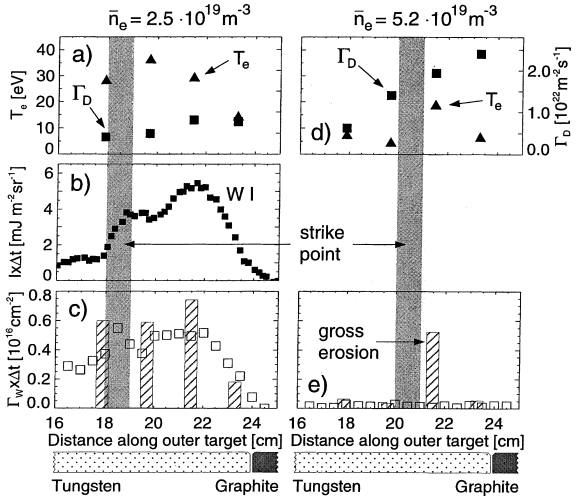

Fig. 4. Radial distribution of gross and net erosion for two series of discharges at different plasma densities. In the high density discharges the plasma was additionally heated with 1.7 MW neutral beam injection. (a) and (d) show the average of Γ_D and T_e over the stationary plasma phases obtained from flush mounted Langmuir probes. (b) shows the radial distribution of the WI intensity in the low-density case. (c) and (e) show the radial distribution of net erosion determined from probes exposed in the respective discharge series and the integrated gross erosion calculated from the Langmuir probe data using an empirical fit to the spectroscopically measured tungsten sputtering yield (Fig. 3). The plate coordinate represents the distance from the inner edge of the outer divertor plate.

position of the flat-top phase can be attributed to the probes integration over the initial plasma phases where the plasma fan has a high temperature and moves outwards from the touch down location to its stationary position.

At four radial positions time resolved values of Γ_D and T_e are provided by Langmuir probes flush mounted in the divertor plate. Fig. 4(a) shows the average over the stationary plasma phase. At the respective positions the time integrated gross erosion flux

$$\Phi_W = \int \Gamma_W \, dt = \int \Gamma_D Y(T_e) dt$$

was calculated using an empirical fit of the spectroscopically determined erosion yield (Fig. 3).

For the low-density discharge [$\bar{n}_e = 2.5 \times 10^{19}$ m^{-3}, Fig. 4(a) and (c)] the measured net erosion is close to the calculated gross erosion. On the other hand, in an Ohmic discharge with higher density [$\bar{n}_e = 5.2 \times 10^{19}$ m^{-3}, Fig. 4(d) and (e)] the observed net erosion is much smaller, just above the detection limit. At the strike-point position the calculated gross erosion, however, exceeds the net erosion by an order of magnitude. The strong reduction of net erosion in this case is attributed to the effect of prompt local redeposition. With increasing plasma density the ionization mean-free-path of sputtered tungsten atoms decreases leading to a corresponding increase of the probability for prompt redeposition within the first gyro orbit after ionization [31]. In addition to the reduced net erosion yield, the lifetime of tungsten components will further benefit from prompt local redeposition due to the short distance between the locations of erosion and redeposition, which is typically in the millimeter range [32] and therefore strongly reduces long-term migration of eroded material by subsequent erosion–redeposition steps. It should be noted that prompt local redeposition is negligible for low-Z elements because their ionization mean-free-path is much longer than the corresponding ion gyro radius for the plasma conditions described above.

Since W-sputtering is dominated by impact of multiply charged impurity ions, it will also be affected by external impurity seeding used for radiative cooling of the edge plasma. The tungsten erosion will, however, be subject to two competing effects. On one hand, the additional impurity ions will cause increased sputtering. On the other hand, the strong decrease of the plasma temperature at the target plates due to the radiation cooling acts in the opposite direction. Both effects have been confirmed experimentally as shown in Fig. 5 [9]. In the discharge with lower divertor density [Fig. 5(b)] the Ne-seeding did not lead to a sufficient drop of the divertor temperature. Consequently the WI emission is strongly increasing with increasing gas puff rate. At higher divertor density and lower initial divertor temperature [Fig. 5(a)] the Ne-seeding does not lead to an increase of the WI intensity. Correspondingly with neon puffing rates at levels where divertor detachment occurred (CDH mode), the WI line emission vanished completely despite the comparatively high Ne ion fraction in the plasma.

5. Migration and global redeposition

While a significant fraction of the eroded tungsten will be redeposited close to the sputter location, in particular at high plasma densities and low temperatures as discussed in Section 4, the remaining ions will be further ionized and eventually reach the main plasma. The probability of this transport process is quantified by the divertor retention capability. As discussed in Section 3, the cross-field transport in the main plasma may change drastically depending on the plasma parameters. Therefore, it is desirable to separate the transport processes in the edge plasma, which are mainly responsible for the divertor retention, from the impurity transport in the confined plasma. A good quantity for the characterization of the divertor retention capability is the ratio

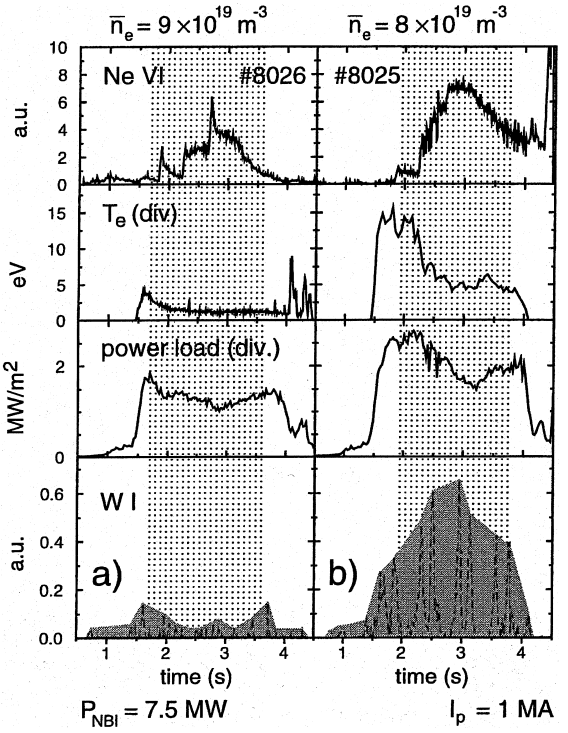

Fig. 5. Effect of Ne seeding on tungsten erosion for two discharges with different divertor temperatures. At low temperatures (a) Ne does not lead to an increase of the WI radiation. At higher divertor temperature (b) the WI line increases strongly corresponding to the Ne-puffing rate.

of the impurity density above the target plates to the impurity density in the mid-plane edge plasma. Unfortunately both quantities are not directly accessible to measurements.

Alternatively, the particle flux crossing the flux surface defined by the ICRH antenna limiters can be used to quantify the edge plasma tungsten density at the mid-plane. This quantity can be obtained from surface analysis of collector probes exposed in the limiter shadow by the mid-plane manipulator system (Fig. 1). Cylindrical probes are covered by a graphite shield with a slit oriented in radial direction. By rotating the probes time resolved data can be obtained. The probe collects W-ions passing through an effective surface area, which is defined by a flux tube extending between ICRH limiter and probe with the poloidal width given by the slit width of the probe shield. The radial deposition profile was found to decrease exponentially with typical decay lengths of 8–12 mm. This explains the absence of significant tungsten deposition at the main vessel surfaces not in direct contact with the plasma. Tungsten ions diffusing into the scrape-off region will be deposited at positions where the magnetic field lines intersect the limiting surfaces.

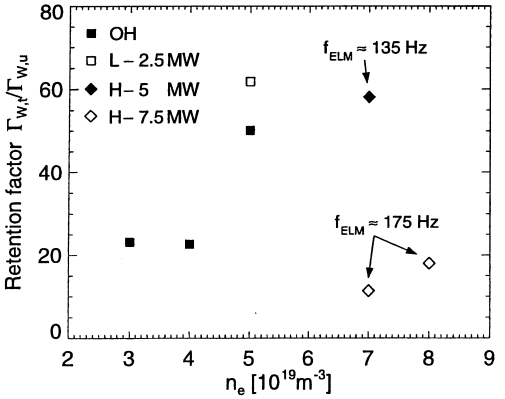

Fig. 6. Ratio of tungsten flux at the outer divertor plate and in the mid-plane edge plasma as a function of the plasma density. The data were obtained by averaging over several data points in the respective density intervals.

By integration over the radial profile of the W-deposition, one obtains the local cross-field flux of W-ions. Assuming a simple model of purely anomalous cross-field diffusion and parallel ion flux reaching target and limiter surfaces with sound speed [33], one can compute an estimate of the tungsten flux in the mid-plane scrape-off layer. Fig. 6 shows the ratio of the spectroscopically measured tungsten flux at the outer divertor plate and the tungsten flux in the mid-plane edge plasma as a function of the plasma density. The retention factor increases with plasma density, which is attributed to the decreasing penetration probability of eroded tungsten atoms and to the correspondingly increasing friction force on tungsten ions directed towards the divertor plates. In H-mode discharges one observes a degradation of the retention factor with increasing heating power. This might be partly explained by increased upstream transport induced by equilibration of the excess pressure, which is built up in the divertor plasma by each ELM.

For quantitative analysis of divertor retention the ratio of upstream density and target plate density can be derived by transport simulations, validated by corresponding W-flux measurements. For the low density Ohmic discharge discussed in Section 4 (Fig. 4(a)–(c)) tungsten transport was modeled by DIVIMP simulations. DIVIMP [34] traces sputtered impurities in a given background plasma assuming classical transport parallel to the magnetic field and anomalous cross-field transport until they are finally redeposited. For the respective discharges the plasma background model was computed by the B2/EIRENE code package [35]. Fig. 7(a) shows the computed tungsten density in the mid-plane edge plasma and just above the outer target plate. From the ratio of the densities (Fig. 7(b)) one obtains a probability of the order 1% for an ionized W-atom to reach

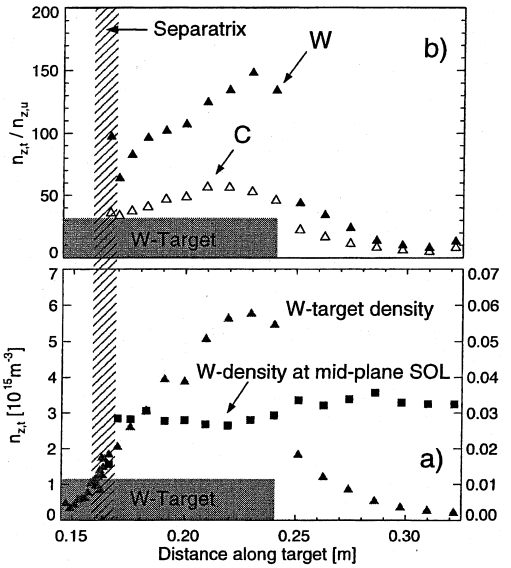

Fig. 7. Radial profiles of tungsten densities at outer target plate and in mid-plane edge plasma, respectively (a). The mid-plane density has been mapped along the respective flux tubes on the target plate coordinates. The radial variation of the retention factor given by the ratio of both quantities is shown in (b) for carbon and tungsten.

the upstream edge plasma. This does not include effects of prompt local redeposition, which will lead to an accordingly lower probability for *sputtered* W-atoms to reach the upstream region. The simulations were also carried out for carbon tiles assuming physical sputtering without chemical erosion effects. In this case the retention capability is reduced by a factor of ≈3 compared to tungsten. The better retention of tungsten can be attributed at least partly to the longer ionization mean-free-path of carbon and the corresponding higher penetration probability of carbon ions into the divertor plasma.

The migration and the redeposition of the eroded tungsten atoms were investigated by ex situ analysis of long-term sample probes and of samples taken from a complete poloidal set of plasma facing components, which were removed after the tungsten divertor campaign.

Proton Induced X-ray Emission (PIXE) was used for tungsten detection [36]. The amount of deposited W-atoms was derived from the integral over the L_β doublet of tungsten at 9.68/9.96 keV.

At the main chamber components a surface contamination level of approximately 2×10^{15} atoms/cm^2 was found without significant variation along the poloidal coordinate [36]. Similar measurements were performed in the previous experimental campaign, where some tungsten covered test tiles had already been in-

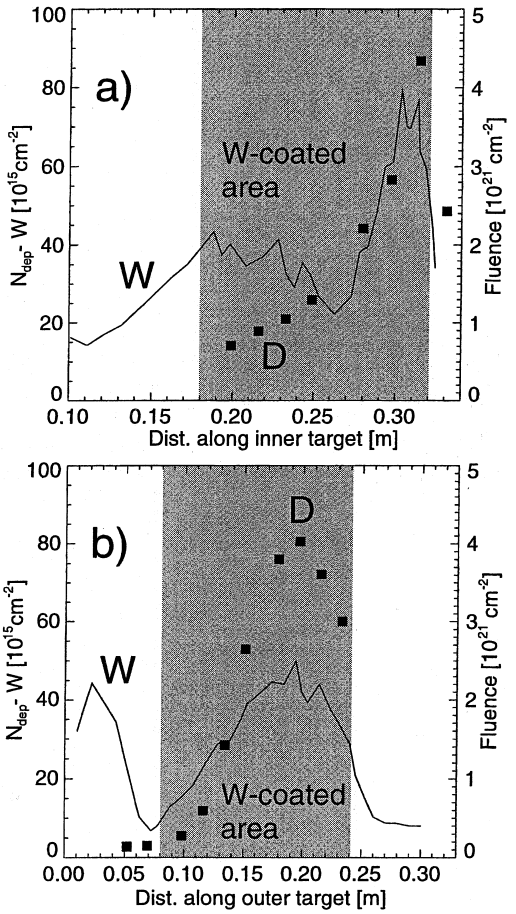

Fig. 8. Correlation of the W-deposition with the total deuterium fluence of the tungsten experimental campaign for inner (a) and outer divertor plate (b).

stalled in the divertor [6]. By comparing the data of the two subsequent campaigns, we infer an upper limit of ≈10^{15} W atoms/cm^2 deposited within the total plasma discharge time of ≈3000 s.

Significantly higher W-deposits exceeding the main chamber deposition by a factor of up to 50–80 were found on the lower divertor plates (Fig. 8). Redeposition in the W-coated region was determined by analyzing graphite tiles of the thermography diagnostics, which could not be replaced by tungsten coated tiles. The maxima of the deposition are closely correlated to the peak values of the deuterium fluence integrated over the whole experimental campaign representing the average strike point position (squares in Fig. 8). For geometric reasons, the strike point position at the inner divertor does not vary as much as at the outer target, which explains the more peaked shape of the deposition at the inner target plate. A similar deposition pattern was found on the graphite target tiles after the previous

experimental campaign with tungsten test tiles employed in the divertor [6].

Visual inspection of the tungsten tiles revealed deposited layers, in particular on the tiles from the inner divertor. The composition of these layers was determined by X-ray Photo-electron Spectroscopy (XPS) and was found to consist (apart from tungsten) of varying fractions of carbon, boron and oxygen [36]. Using 2 MeV proton RBS the depth distribution of tungsten could be determined by a simplified analysis representing the low-Z fractions by pure carbon. The resulting depth profiles of tungsten at the average strike point locations of inner and outer target plates are shown in Fig. 9 for the shadowed region and the plasma wetted area, respectively. At the outer divertor the fraction of tungsten was found to be close to the initial level indicating dominance of erosion over deposition. In contrast, the low-Z deposits at the inner divertor reached a level corresponding to a thickness of up to 5 μm with only a few percent tungsten remaining at the surface. Detailed analysis of the shadowing effects due to the tilted surfaces [36] shows that the deposition at the inner target plate is closely correlated to the incident particle fluence. The different behaviour of inner and outer divertor is in good agreement with TRIM simulations of the tungsten erosion and corresponding surface modification by simultaneous bombardment with deuterium and carbon ions [30,37]. The dominance of deposition at the inner target plate can be attributed to the lower average temperature compared to the outer divertor plate [36].

6. Hydrogen isotope retention

Apart from the influence of the eroded W-atoms on plasma performance, the retention of hydrogen isotopes in the tungsten material may also affect plasma operation, in particular with respect to the possible formation of tritium inventories. Near surface inventories of deuterium in the tungsten tiles were determined ex situ by nuclear reaction analysis (NRA) using the reaction $^3He + D \rightarrow p + \alpha$ [36]. With 790 keV energy of the incident beam, deuterium can be detected to depths of up to 1 μm. The total inventory of hydrogen and deuterium was determined by thermo-controlled desorption spectroscopy (TDS) [38].

Detailed investigation of the tungsten tiles [39] revealed about one order of magnitude larger D-inventories at the inner tiles than at the outer tiles as shown in Fig. 10 (a) and (b), which is in accordance to the layers of low-Z material observed at those tiles. We conclude that the inventories are strongly dominated by co-deposition mainly with carbon. The much lower inventories at the outer W-tiles are attributed to implantation of deuterium because in the outer divertor erosion prevails due to the higher average electron temperature [36]. The similar values of the D-inventory obtained by TDS and the near surface inventory measured by NRA proves that retention of hydrogen isotopes in the tungsten bulk material is negligible in contrast to data found for graphite target tiles as illustrated in Fig. 10(c) [39].

Therefore, hydrogen inventories might be greatly reduced by using tungsten as plasma facing material. This benefit, however, might be partially lost by simultaneous use of low-Z material for other plasma facing components leading to formation of hydrogen inven-

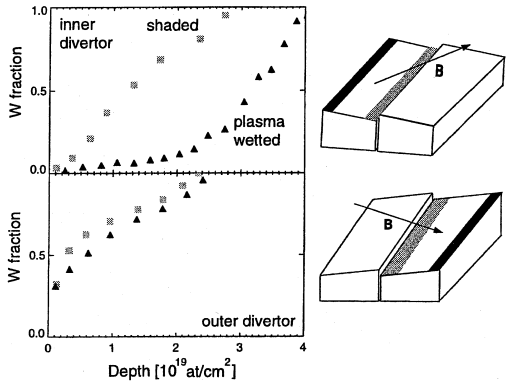

Fig. 9. Depth profile of tungsten in strike point zones of inner and outer target plate after the experimental campaign.

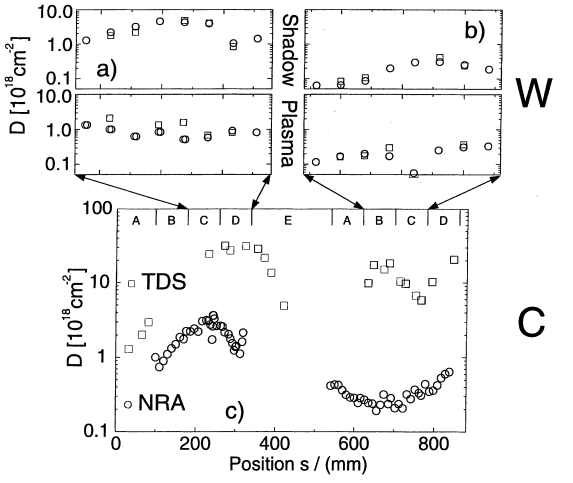

Fig. 10. Near surface D-inventory measured by NRA and total D-inventory from TDS analysis across inner (a) and outer (b) tungsten tiles. For graphite (c), near-surface NRA data refer to the same experimental period (graphite thermography tiles). The corresponding TDS data were obtained from graphite tiles removed after the previous experimental campaign and refer to three subsequent campaigns.

tories by co-deposition at deposition dominated surfaces [40].

7. Summary

Tungsten target tiles were successfully used at the strike point areas of the ASDEX Upgrade Divertor I configuration for a full experimental campaign.

Global plasma parameters remained unchanged compared to respective results of previous campaigns with graphite divertor plates. The introduction of tungsten divertor tiles did not lead to any significant degradation of plasma performance. In about 85% of the discharges the tungsten concentration in the main plasma remained below the limit of 2×10^{-5} considered as critical for fusion devices featuring ignited plasmas. Under a few specific discharge conditions promoting general impurity accumulation, tungsten accumulated as well leading to plasma contamination clearly above the limit of 2×10^{-5}.

Divertor retention of tungsten was found to improve with increasing plasma density whereas in H-mode scenarios degradation of the divertor retention capability occurred with increasing heating power. Simulation of tungsten and carbon transport for Ohmic discharge conditions revealed a better divertor retention factor for tungsten exceeding the carbon retention by a factor of approximately three.

The plasma–surface interaction of the tungsten tiles turned out to be strongly dominated by low-Z impurities, in particular by the carbon eroded from graphite plasma facing components in the main chamber.

The carbon impurity concentration in the plasma did not change significantly by the replacement of the previous graphite divertor tiles with tungsten tiles. Therefore, we can conclude that the main sources for carbon are not due to erosion of the divertor tiles.

Tungsten erosion is dominated by impact of multiply charged low-Z impurity ions. The measured erosion yields are well described by a model assuming sputtering by simultaneous bombardment with D and C where the deuterium contributes only by the continuous removal of deposited carbon. At high divertor densities the net erosion is significantly reduced by prompt local redeposition. While external impurity seeding might lead to increased sputtering at high divertor temperatures, in scenarios with radiative cooling and corresponding divertor detachment tungsten erosion turned out to be clearly below the detection limit.

Hydrogen retention in tungsten will lead to much lower inventories as expected for codeposition with carbon or beryllium. From the observed low-Z deposition pattern, we conclude that in devices where tungsten is used in conjunction with low-Z materials, the W-surface in deposition dominated zones will be quickly covered by deposited layers of the respective low-Z atoms. Due to the in–out asymmetry of the divertor power load such conditions will mainly be found in the inner divertor of tokamaks.

After the tungsten divertor campaign, the Divertor I configuration of ASDEX Upgrade was replaced by a new design with vertical Lyra shaped target plates. Because much higher heat loads compared to Divertor I were expected from the addition of a second NBI injector, carbon fibre compounds were selected as target plate material for the strike point region. Based on the positive experience with tungsten target tiles, replacement of the graphite baffle modules at the divertor throat by tungsten coated material as in the ITER design is a promising option for future experimental campaigns. Vapor deposition of tungsten on the graphite tiles of the inner heat shield could be a possibility to effectively reduce the corresponding carbon source.

References

[1] V. Arunasalam, C. Barnes, K. Bol, K. Brau, N. Bretz, et al., in: Proc. Eighth Europ. Conf. on Contr. Fusion and Plasma Phys., Prague 1977, vol. II, 1978, pp. 17–28.
[2] K. Bol, V. Arunasalam, M. Bitter, D. Boyd, K. Brau et al., in: Plasma Physics and Controlled Nuclear Fusion Research 1978, vol. 1, IAEA, Vienna, 1979, p. 11.
[3] M. Tokar, J. Rapp, G. Bertschinger, L. Könen, H. Koslowski et al., Nucl. Fusion 37 (1997) 1691.
[4] J. Rapp, M. Tokar, L. Könen, H. Koslowski et al., Plasma Phys. Controlled Fusion 39 (1997) 1615.
[5] K. Krieger, J. Roth, A. Annen, W. Jacob, C.S. Pitcher et al., J. Nucl. Mater. 241–243 (1997) 684.
[6] K. Krieger, V. Rohde, R. Schwörer, K. Asmussen, C. García-Rosales et al., J. Nucl. Mater. 241–243 (1997) 734.
[7] K. Krieger, K. Asmussen, R. Neu, V. Rohde, J. Roth et al., in: Plasma Physics and Controlled Nuclear Fusion Research 1996, vol. 1, IAEA, Vienna, 1997, pp. 817–823.
[8] K. Krieger, H. Maier, V. Rohde, K. Asmussen, M. Balden et al., in: M. Schittenhelm, R. Bartiromo, F. Wagner (Eds.), Proc. of The 24th EPS Conference on Controlled Fusion and Plasma Physics, Berchtesgaden, 1997, Europhysics Conference Abstracts, vol. 21A, Part IV, EPS, Petit-Lancy, 1997, pp. 1421–1424.
[9] A. Thoma, K. Asmussen, R. Dux, K. Krieger, A. Herrmann et al., Plasma Phys. Controlled Fusion 39 (1997) 1487.
[10] A. Thoma, K. Asmussen, R. Dux, K. Krieger, A. Herrmann et al., in: M. Schittenhelm, R. Bartiromo, F. Wagner (Eds.), Proc. of The 24th EPS Conference on Controlled Fusion and Plasma Physics, Berchtesgaden, 1997, Europhysics Conference Abstracts, vol. 21A, Part IV, EPS, Petit-Lancy, 1997, pp. 1409–1412.
[11] R. Neu, K. Asmussen, S. Deschka, A. Thoma, M. Bessenrodt-Weberpals et al., J. Nucl. Mater. 241–243 (1997) 678.
[12] R. Neu, K. Asmussen, K. Krieger, A. Thoma, H.-S. Bosch et al., Plasma Phys. Controlled Fusion 38 (1996) A165.

[13] R. Neu et al., to be published in Nucl. Fusion.
[14] C. García-Rosales, S. Deschka, W. Hohenauer, R. Duwe, E. Gauthier et al., Fusion Tech. 32 (1997) 263.
[15] S. Deschka, C. García-Rosales, W. Hohenauer, R. Duwe, E. Gauthier et al., J. Nucl. Mater. 233–237 (1996) 645.
[16] H. Maier, S. Kötterl, K. Krieger, R. Neu, M. Balden, ASDEX Upgrade Team, J. Nucl. Mater. 258–263 (1998) 921.
[17] A. Kallenbach, R. Neu, W. Poschenrieder, ASDEX Upgrade Team, Nucl. Fusion 34 (1994) 1557.
[18] K. Asmussen, K. Fournier, J. Laming, R. Neu, J. Seely et al., Nucl. Fusion 38 (1998) 967.
[19] K. Asmussen, R. Neu, R. Dux, W. Engelhardt, K. Fournier et al., in: M. Schittenhelm, R. Bartiromo, F. Wagner (Eds.), Proc. of The 24th EPS Conference on Controlled Fusion and Plasma Physics, Berchtesgaden, 1997, Europhysics Conference Abstracts, vol. 21A, Part IV, EPS, Petit-Lancy, 1997, pp. 1393–1396.
[20] R. Neu, K.B. Fournier, D. Schlögl, J. Rice, J. Phys. B 30 (1997) 5057; preprint in IPP 10/7, June 1997.
[21] G. Fussmann, J. Hofmann, G. Janeschitz, K. Krieger, E. Müller et al., J. Nucl. Mater. 162–164 (1989) 14.
[22] G. Fussmann, A. Kallenbach, K. Krieger, K. Steuer, in: Controlled Fusion and Plasma Heating, Europhysics Conference Abstracts, vol. 14B, Part III, 1990, p. 1423.
[23] R. Dux, K. Asmussen, R. Neu, S. de Peña Hempel, V. Rohde et al., in: M. Schittenhelm, R. Bartiromo, F. Wagner (Eds.), Proc. of The 24th EPS Conference on Controlled Fusion and Plasma Physics, Berchtesgaden, 1997, Europhysics Conference Abstracts, vol. 21A, Part IV, EPS, Petit-Lancy, 1997, pp. 1405–1408.
[24] A.R. Field, J. Fink, R. Dux, G. Fussmann, U. Schumacher et al., Rev. Sci. Instrum. 66 (1995) 5433.
[25] J. Steinbrink, Spektroskopische Untersuchungen von zerstäubtem Wolfram in einer linearen Plasmaanlage, Master's Thesis, Humbold-Universität zu Berlin, 1997.
[26] J. Steinbrink, U. Wenzel, W. Bohmeyer, G. Fussmann, and the PSI-Team, in: Proc. 24th EPS Conf. Contr. Fus. and Plasma Physics, Europhysics Conference Abstracts, vol. 21A, Part IV, 1997, p. 1809.
[27] A. Geier, K. Asmussen, A. Bard, R. Neu, K. Krieger et al., A sublimation Probe for the Injection of High-Z Impurities into Fusion Devices, to be published in Rev. Sci. Instrum.
[28] M. Weinlich, A. Carlson, Plasma Phys. 4 (1997) 2151.
[29] W. Eckstein, K. Krieger, J. Roth, J. Nucl. Mater. 258–263 (1998) 912.
[30] D. Naujoks, W. Eckstein, J. Nucl. Mater. 230 (1996) 93.
[31] D. Naujoks, K. Asmussen, M. Bessenrodt-Weberpals, S. Deschka, R. Dux et al., Nucl. Fusion 36 (1996) 671.
[32] D. Naujoks, J. Roth, K. Krieger, G. Lieder, M. Laux, J. Nucl. Mater. 210 (1994) 43.
[33] P. Stangeby, G. McCracken, Nucl. Fusion 30 (1990) 1225.
[34] P. Stangeby, J. Elder, J. Nucl. Mater. 196–198 (1992) 258.
[35] D.P. Coster, R. Schneider, J. Neuhauser, H.-S. Bosch, R. Wunderlich et al., J. Nucl. Mater. 241–243 (1997) 690.
[36] H. Maier, K. Krieger, M. Balden, J. Roth, ASDEX Upgrade Team, these Proceedings.
[37] D. Naujoks, W. Eckstein, J. Nucl. Mater. 220–222 (1995) 993.
[38] P. Franzen, H. Maier, D. Schleußner, R. Behrisch, M. Balden et al., in: Controlled Fusion and Plasma Physics, Europhysics Conference Abstracts, vol. 21A, Part IV, 1997, p. 1429.
[39] D. Schleußner, H. Maier, P. Franzen, R. Behrisch, M. Balden, et al., these Proceedings.
[40] M. Mayer, R. Behrisch, H. Plank, J. Roth, G. Dollinger et al., J. Nucl. Mater. 230 (1996) 67.